

Lagrangian Space Nonlinear E -mode clustering

Hao-Ran Yu,^{1,2} Ue-Li Pen,^{2,3,4,5} and Hong-Ming Zhu^{6,7}

¹*Kavli Institute for Astronomy and Astrophysics, Peking University, Beijing 100871, China*

²*Canadian Institute for Theoretical Astrophysics, University of Toronto,
60 St. George Street, Toronto, Ontario M5S 3H8, Canada*

³*Dunlap Institute for Astronomy and Astrophysics, University of Toronto,
50 St. George Street, Toronto, Ontario M5S 3H4, Canada*

⁴*Canadian Institute for Advanced Research, CIFAR Program in Gravitation and Cosmology, Toronto, Ontario M5G 1Z8, Canada*

⁵*Perimeter Institute for Theoretical Physics, 31 Caroline Street North, Waterloo, Ontario, N2L 2Y5, Canada*

⁶*Key Laboratory for Computational Astrophysics, National Astronomical Observatories,
Chinese Academy of Sciences, 20A Datun Road, Beijing 100012, China*

⁷*University of Chinese Academy of Sciences, Beijing 100049, China*

(Dated: October 13, 2016)

We study the nonlinear E -mode clustering in Lagrangian space by using large scale structure (LSS) N -body simulations and use the displacement field information in Lagrangian space to estimate the primordial linear density field. We find that, compared to Eulerian nonlinear density fields, the negative divergence of E -mode displacement fields in Lagrangian space improves the cross-correlation with initial density field by factor of $6 \sim 7$, containing 2 orders of magnitude more primordial information. In reality, the displacement field is dominated by linear evolution and insensitive of nonlinear shell-crossing, vorticity or baryonic physics, and thus can be stably solved from only the final matter distributions. This illustrates ability of potential reconstruction algorithms, to reconstruct baryonic acoustic oscillation (BAO) from current and future large scale structure surveys.

I. INTRODUCTION

Our universe starts from primordial Gaussian perturbations at a very early stage, and from those fluctuations, the gravitational instability drives the formation of the large scale structure (LSS) distribution of matter [1, 2]. These structures grow linearly until the perturbations are large enough so that the first order perturbation theories are unable to analytically describe the LSS distributions [3]. As a result, the final nonlinear LSS distribution contains higher order statistics, and thus makes it more challenging to be interpreted into basic cosmological parameters. One such example is that, the baryonic acoustic oscillation (BAO) scale can be used as a “standard ruler” to constrain the cosmic expansion history and thus probes the dark energy properties [4], but nonlinear evolution smears the BAO features and lowers the measurement accuracy [5, 6]. There are various attempts to recover earlier stages of LSS, in which statistics are closer to Gaussian [7, 8]. Because Gaussian fields can be adequately described by two-point statistics, ideally after some recovery algorithms, more information can be extracted, more straightforwardly, by power spectra or two-point correlation functions [9, 10].

Standard BAO reconstruction algorithms smooth the nonlinear density field on linear scale (~ 10 Mpc/ h) and reverse the large scale bulk flows by a negative Zel’dovich linear displacement [11–13]. Here we propose a new reconstruction method that uses the nonlinear displacement field to recover the primordial density field. In the linear Lagrangian perturbation theory, the negative divergence of the displacement field $\Psi(\mathbf{q})$ respect to Lagrangian coordinates \mathbf{q} gives the linear density field [14]. Of course, the full displacement field $\Psi(\mathbf{q})$ is non-observable, as it requires the initial distributions of matter, however there are many techniques to estimate the nonlinear displacement field from a final distribution of matter. For example, when a homogeneous initial matter distribution is assumed, there is a unique solution of curl-less displacement

field to relate the initial and final distributions without shell-crossing. This solution can be solved by a metric transformation equation [15, 16]. In 1-dimensional (1D) case, the exact solution of [15] simplifies to an ordering of matter elements by Eulerian coordinates. Zhu *et al.* [17] apply this algorithm to the result of an 1D simulation [3] and obtain an estimated displacement field $\tilde{\Psi}(\mathbf{q})$, and find that this new method well recovers the linear information and reconstructs BAO peak in correlation function. In 3D case, there are various techniques to obtain $\tilde{\Psi}(\mathbf{q})$. However one needs to carefully consider effects of curl, shell-crossing in 3D case.

Before these steps, we need to quantify the amount of linear information that can be recovered from the full nonlinear displacement field $\Psi(\mathbf{q})$, and further estimations $\tilde{\Psi}(\mathbf{q})$ can be compared with this result. In this paper we run a LSS N -body simulation and track the motion of particles to obtain $\Psi(\mathbf{q})$. According to this we reconstruct the linear density field and compare to the primordial density field of the initial conditions. We describe the simulation and reconstruction algorithm in section II, and we show the results in section III. Discussion and conclusion are in section IV.

II. METHOD

We show the LSS simulation and displacement field setups in section II A, and the reconstruction processes are presented in section II B.

A. Simulation

We use the open source cosmological simulation code CUBE [18]. Cosmological parameters are set as $\Omega_m = 0.27$, $\Omega_\Lambda = 0.73$, $h_0 = 0.68$, $n_s = 0.96$ and $\sigma_8 = 0.83$. Initial conditions are gen-

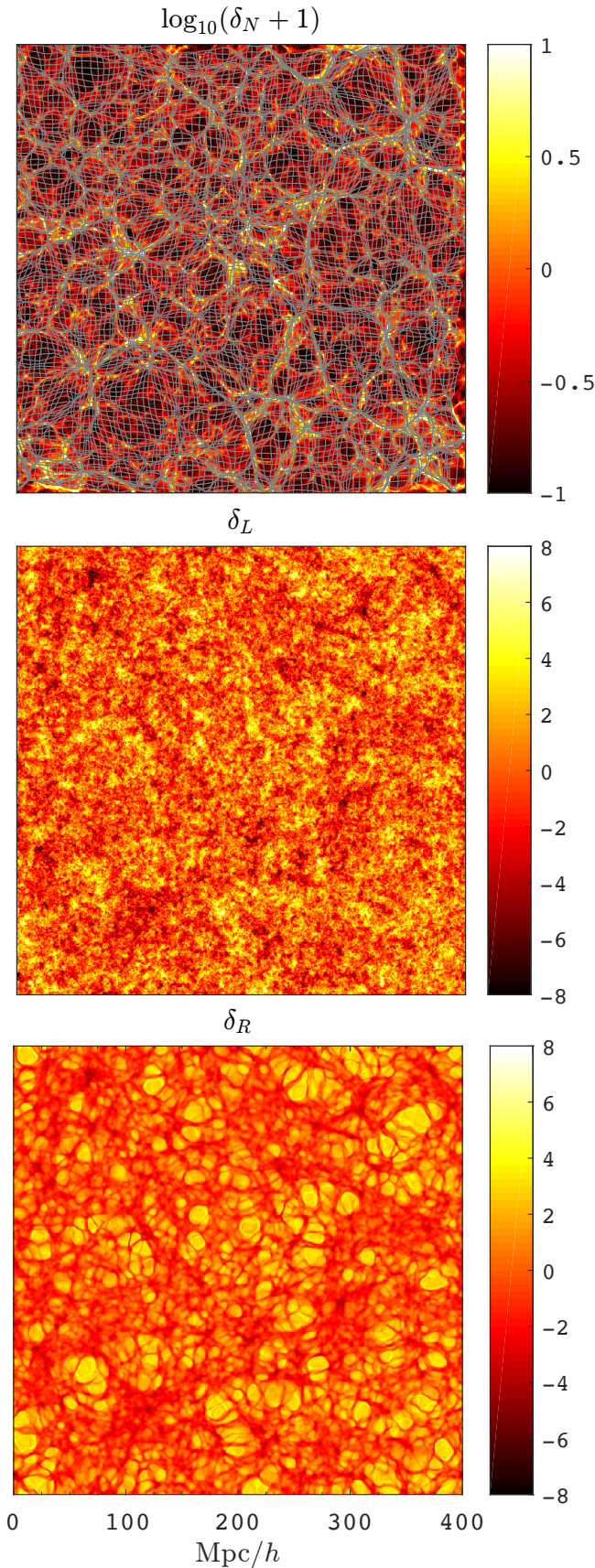


FIG. 1. Visualization of the nonlinear density field δ_N (top), linear density field δ_L (middle) and the raw reconstructed density field δ_R (bottom). These projections have $9.375 \text{ Mpc}/h$ thickness and $400 \text{ Mpc}/h$ per side. The top panel shows the nonlinear displacement field Ψ by the deformed mesh, which traces the LSS of δ_N .

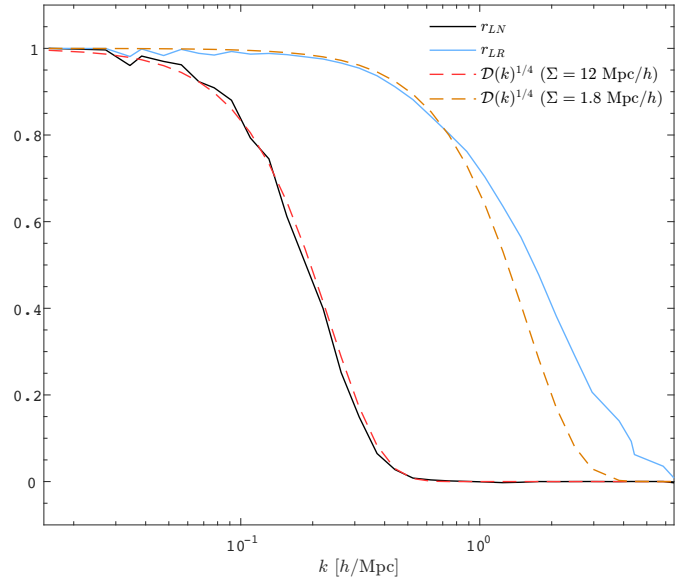


FIG. 2. Correlation functions $r(\delta_L, \delta_N)$ and $r(\delta_L, \delta_R)$ (solid lines) and their scaled BAO damping models (dotted lines).

erated at redshift $z = 50$ using Zel'dovich approximation, and using a CLASS transfer function. $N_p = 512^3$ N -body particles are evolved via their mutual gravitational interactions to $z = 0$, in a periodic box with $L = 400 \text{ Mpc}/h$ per side. The code is set to use standard a particle-mesh (PM) algorithm [19] on a two-level mesh grids (details see [20]) and cloud-in-cell (CIC) is used in particle interpolations in force calculation and obtaining the density field $\rho(\mathbf{x})$ in Eulerian coordinates \mathbf{x} at late stages. We use density contrast $\delta \equiv \rho/\langle\rho\rangle - 1$ to describe the density fluctuations. The primordial linear density field δ_L is given by the initial stage and scaled to $z = 0$ by the linear growth factor. In the top and middle panels of Fig.1 we show projections of the nonlinear density field δ_N given by the simulation and the linear density field δ_L . δ_N is obtained by the particle distribution at redshift $z = 0$, and the particles are interpolated by using the cloud-in-cell (CIC) algorithm. Because δ_N is highly nonlinear and follows an approximate log-normal distribution, we plot $\log_{10}(\delta_N + 1)$ instead. The nonlinear evolution of δ_N makes it very different from δ_L in appearance.

The two-point statistics of these density fields are quantified by the cross power spectrum $P_{ij}(k) \equiv (2\pi)^{-3} \langle |\delta_i(k)| |\delta_j(k)| \rangle$, where subscripts i, j may refer to linear (L), nonlinear (N), or reconstructed (R) density fields. When $i = j$ it reduces to the auto power spectrum $P_{ii}(k)$ or $P(k)$. We usually plot the dimensionless power spectrum $\Delta^2(k) \equiv k^3 P(k)/2\pi^2$.

B. Reconstruction

In the simulation, we use particle-ID (PID) to record the initial (Lagrangian) location \mathbf{q} of particles, and the information is tracked until the $z = 0$ and we can get the Lagrangian displacement vector $\Psi \equiv \mathbf{x} - \mathbf{q}$ for every particle. Then these vectors are interpolated onto the initial Lagrangian coordinates \mathbf{q} of particles and we get the displacement field $\Psi(\mathbf{q})$. To visualize the Ψ

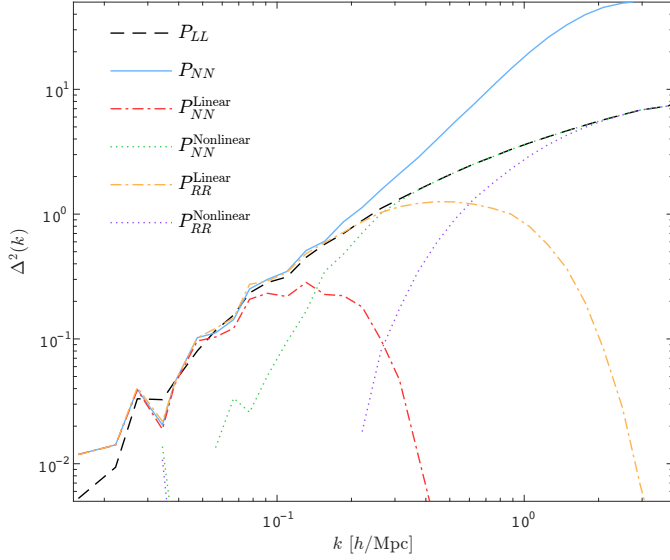


FIG. 3. Power spectra decomposition of density fields and their filtered density field.

field, we draw a 3D uniform mesh over the volume, and use the given Ψ field to deform the mesh according to the direction and physical amplitude of Ψ . In the top panel of Fig.1, The resulting mesh illustrates a pseudo “curvilinear coordinate” similar to [15], however the mesh can be overlapped due to shell-crossing. The densest mesh grids trace the densest structures of δ_N , whereas the undeformed grid positions are the Lagrangian coordinates in which we do the reconstruction. The raw reconstructed density field is given by the differential motion of matter elements,

$$\delta_R = -\nabla \cdot \Psi(\mathbf{q}). \quad (1)$$

Because the reconstruction processes are implemented on Lagrangian coordinates, δ_R takes the coordinates of \mathbf{q} instead of \mathbf{x} . We just write \mathbf{q} 's Fourier wave number k_q as k to simplify the expression.

To quantify the linear information in the reconstructed density field, we decompose δ_R in Fourier space as

$$\delta_R(k) = r' \delta_L + \delta_N, \quad (2)$$

where $r' \delta_R$ is completely correlated with linear density δ_L . Correlating equation (2) with δ_L gives

$$P_{LR} = r' P_{LL} + P_{LN}, \quad (3)$$

where $P_{ij} \equiv \langle \delta_i \delta_j \rangle$ denotes the cross power spectrum. Since δ_N is uncorrelated with δ_L , $P_{LN} = 0$. With the definition of cross correlation coefficient $r(\delta_L, \delta_R) \equiv P_{LR} / \sqrt{P_{LL} P_{RR}}$ and bias $b^2 = P_{RR} / P_{LL}$, we solve $r' = P_{LR} / P_{LL} = r b$. We plot the cross correlation coefficient r_{LN} and r_{LR} in Fig.2. Clearly, δ_R contains much more linear information on smaller scales.

According to equation (2), the auto power spectrum is decomposed as

$$P_{RR} = r^2 b^2 P_{LL} + P_{NN}, \quad (4)$$

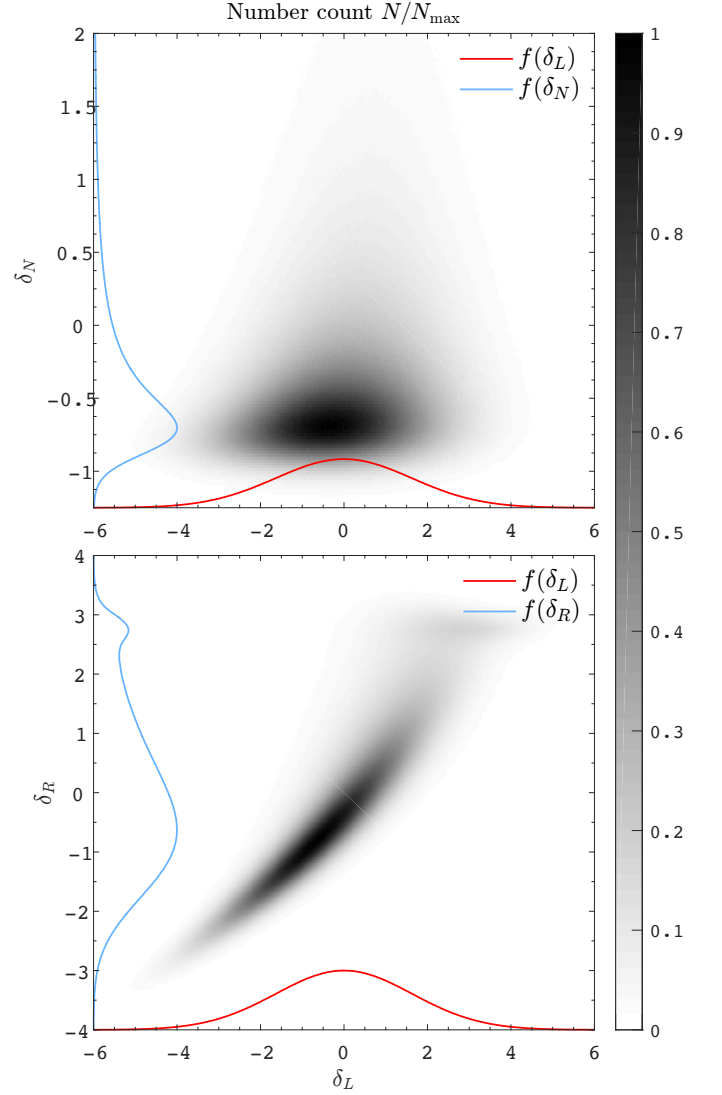


FIG. 4. 2D-PDF (preliminary)

and $P_{NN} = (1 - r^2) P_{RR}$. Then we construct a Wiener filter to filter out the uncorrelated part in δ_R :

$$W(k) = \frac{r^2 b^2 P_{LL}}{r^2 b^2 P_{LL} + P_{NN}} = r^2. \quad (5)$$

The Wiener filters are also plot in Fig.2. The estimated linear density, or the optimal reconstructed density is given by

$$\tilde{\delta}_R = W b^{-1} \delta_R. \quad (6)$$

The optimal reconstructed power spectrum is given by

$$\tilde{P} = W^2 b^{-2} P_{RR} = W^2 P_{LL} + W^2 b^{-2} P_{NN}. \quad (7)$$

The W^2 describes the damping of the linear power spectrum.

III. RESULTS

From the above algorithm, the projection of δ_R is plotted in the bottom panel of Fig.1, which looks closer to δ_N . In the top panel of Fig.3, the blue solid and black dashed curves show the auto power spectra of nonlinear density field δ_N and δ_L . Their difference shows the nonlinear evolution of LSS on small scales. Their cross power drops to a very low value, indicating a loss of linear information in the nonlinear power spectrum. In the bottom panel of Fig.3 we show the auto power spectrum of δ_R and its cross power with δ_L . Despite of a lowered power of δ_R compared to δ , it has a much higher cross power with δ_L compared to δ_N , up to a relatively smaller scale (higher k).

Fig.2 shows the cross correlation functions, damping factors $W^2(k)$ for the optimal filtered nonlinear and reconstructed density fields. We can see that the cross correlation r_{LR} is recovered to nearly an order of magnitude smaller scales compared to r_{LN} . We also fit the Gaussian BAO damping model $\mathcal{D}(k) = \exp(-k^2 \Sigma^2/2)$ and give $\Sigma = 1.8 \text{ Mpc}/h$ and $\Sigma = 12 \text{ Mpc}/h$ for reconstructed and nonlinear fields. We repeat the analysis with various box sizes, and the results are consistent.

In the two panels of Fig.3 we show the power spectrum decomposition by equation (4) for both δ_N (with subscripts “ R ” replaced by “ N ”) and δ_R . In the top panel, on scales $k > 0.2 \text{ h}/\text{Mpc}$, P_{NN} term dominates the power spectrum due to a low correlation between δ_L and δ_N . The optimal filtered power spectrum damps quickly on small scales. In comparison, in the bottom panel, P_{NN} starts to dominate on scales $k > 1 \text{ h}/\text{Mpc}$. As a result, the optimal filtered reconstructed power spectrum (by equation (7)) is much higher.

In Fig.4 we use the probability distribution as functions of (δ_L, δ_N) and (δ_L, δ_R) to show the point-point correlation between these two pairs of density fields. In the top panel, δ_N shows an approximate log-normal distribution, and shows no correlation with δ_L . Although δ_L and δ_N have correlations on linear scales (Fig.2), they have no correlation in real space, because initial density fluctuations in Lagrangian coordinates are evolved/transformed to Eulerian coordinates. As the reconstruction is done in Lagrangian space, it recovers certain amount of correlation as shown in the bottom panel of Fig.4. One can also see that δ_R follows a much closer Gaussian distribution. We notice that the less-dense regions of δ_L are more correlated with δ_R , whereas denser regions of δ_L are reconstructed worse, and δ_R shows more dispersion. This is caused by nonlinear effects and it damps out in higher redshifts.

IV. DISCUSSION AND CONCLUSION

We extract the actual displacement field of matter elements in cosmological N -body simulations, and use this displacement

field in Lagrangian coordinates to reconstruct the primordial linear perturbations. The result shows a prominent improvement from r_{LN} to r_{LR} in Fig.2 – recovering the lost linear information on nearly an order of magnitude smaller scales. This is achieved by implementing differential movement information of matter elements on Lagrangian coordinates, rather than on Eulerian coordinates. This result illustrates the feasibility of using estimated displacement field $\tilde{\Psi}(\mathbf{q})$ to reconstruct primordial linear density field. A straightforward example of a estimation of $\tilde{\Psi}(\mathbf{q})$ is given by [15, 16]. In reality, one needs to consider all aspects including vorticity, shell-crossing, bias, noise and data complexities. The impact of these factors can be quantitatively compared with the impact of different estimation methods, and with the exact solution by N -body simulations.

The advantage of using displacement field in reconstruction is its insensitive response from highly nonlinearities – densest regions form because matter elements, after shell crossing, stop experiencing the linear extrapolated of Zel’dovich approximation. i.e. the displacement fields are dominated by early stage linear processes, which is the Lagrangian-Eulerian coordinate transform, while late stage shell-crossing, nonlinear and baryonic processes only fine-tunes the final position \mathbf{x} . In contrast, traditional treatments in reconstruction deals directly on density fields which sensitively relies on nonlinear processes – density values can vary by orders of magnitude due to nonlinear/baryonic physics and many sources of errors.

ACKNOWLEDGEMENTS

We thank Pengjie Zhang for helpful discussions which triggered the inspiration of the work. HRY acknowledges General Financial Grant No.2015M570884 and Special Financial Grant No.2016T90009 from the China Postdoctoral Science Foundation. [ZHM’s acknowledgements.] The Dunlap Institute is funded through an endowment established by the David Dunlap family and the University of Toronto. Research at the Perimeter Institute is supported by the Government of Canada through Industry Canada and by the Province of Ontario through the Ministry of Research & Innovation.

[1] Y. B. Zel’dovich, A&A5, 84 (1970).
 [2] M. Davis, G. Efstathiou, C. S. Frenk, and S. D. M. White, ApJ292, 371 (1985).

[3] M. McQuinn and M. White, J. Cosmology Astropart. Phys.1, 043 (2016), 1502.07389.
 [4] D. J. Eisenstein, New Astronomy Reviews 49, 360 (2005).
 [5] D. J. Eisenstein *et al.*, ApJ633, 560 (2005), astro-ph/0501171.

- [6] W. Ngan, J. Harnois-Déraps, U.-L. Pen, P. McDonald, and I. MacDonald, *MNRAS***419**, 2949 (2012), 1106.5548.
- [7] D. H. Weinberg, *MNRAS***254**, 315 (1992).
- [8] J. Harnois-Déraps, H.-R. Yu, T.-J. Zhang, and U.-L. Pen, *MNRAS***436**, 759 (2013), 1205.4989.
- [9] C. D. Rimes and A. J. S. Hamilton, *MNRAS***360**, L82 (2005), astro-ph/0502081.
- [10] H.-R. Yu, J. Harnois-Déraps, T.-J. Zhang, and U.-L. Pen, *MNRAS***421**, 832 (2012), 1012.0444.
- [11] D. J. Eisenstein, H.-J. Seo, E. Sirko, and D. N. Spergel, *ApJ***664**, 675 (2007), astro-ph/0604362.
- [12] Y. Noh, M. White, and N. Padmanabhan, *Phys. Rev. D***80**, 123501 (2009), 0909.1802.
- [13] N. Padmanabhan, M. White, and J. D. Cohn, *Phys. Rev. D***79**, 063523 (2009), 0812.2905.
- [14] D. Jeong, *Cosmology with high ($z > 1$) redshift galaxy surveys*, PhD thesis, University of Texas at Austin, 2010.
- [15] U.-L. Pen, *ApJS***100**, 269 (1995).
- [16] U.-L. Pen, *ApJS***115**, 19 (1998), astro-ph/9704258.
- [17] H.-M. Zhu, U.-L. Pen, and X. Chen, *ArXiv e-prints* (2016), 1609.07041.
- [18] H. R. Yu and U.-L. Pen, *in prep.* (2016).
- [19] R. W. Hockney and J. W. Eastwood, *Computer simulation using particles* (, 1988).
- [20] J. Harnois-Déraps *et al.*, *MNRAS***436**, 540 (2013), 1208.5098.